Planar Optical Waveguide Temperature Sensor Based on Etched Bragg Gratings Considering Nonlinear Thermo-optic Effect

Sang-Mae Lee
Center for Microelectronic Sensors and MEMS, Department of Electrical & Computer Engineering and Computer Science, University of Cincinnati
Kook-Chan Ahn*†
Department of Mechanical Design Engineering, Chinju National University
Jim S. Sirkis
Smart Materials and Structures Research Center, Department of Mechanical Engineering, University of Maryland

This paper demonstrates the development of optical temperature sensor based on the etched silica-based planar waveguide Bragg grating. Topics include design and fabrication of the etched planar waveguide Bragg grating optical temperature sensor. The typical bandwidth and reflectivity of the surface etched grating has been ~0.2 nm and ~9 %, respectively, at a wavelength of ~1552 nm. The temperature-induced wavelength change is found to be slightly non-linear over ~200 ℃ temperature range. Typically, the temperature-induced fractional Bragg wavelength shift measured in this experiment is 0.0132 nm/℃ with linear curve fit. Theoretical models with nonlinear temperature effect for the grating response based on waveguide and plate deformation theories agree with experiments to within acceptable tolerance.

Key Words : Etched Bragg Grating, Planar Light Waveguide, Butt Coupling Technique, Nonlinear Thermooptic Effect, Temperature Sensor, Classical Lamination Theory

1. Introduction

High-temperature strain measurements are critical to understanding constitutive properties of new high-temperature materials such as metal matrix composites (MMCs), ceramic matrix composites (CMCs), and carbon/carbon composites (CCCs), as well as for determining the mechanical reliability of components produced from these materials. These materials are finding greater use in applications involving advanced aeropropulsion systems and high speed civil transport. Strain gages most commonly used in high temperature measurements are resistance based foil strain gages (Wu et al., 1981 ; Hudson, 1989 ; Stange, 1983 ; Lei et al., 1989) or capacitance based strain gages (Harting, 1975 ; Noltingk, 1974 ; Norris and Yeakley, 1976) and are all limited operating temperature of less than ~850 ℃. The recent entry in high temperature strain sensing field are transducers based on cylindrical optical waveguides (optical fibers) produced from amorphous silica (Chang et al., 1994 ; Lee and Taylor, 1991) and sapphire (Dils, 1983 ; Wang et al., 1992). Silica based optical fiber sensors have been demonstrated up to 1200 ℃, while sapphire-based sensors have been demonstrated in temperature regimes near 1700 ℃. While sapphire sensors are attractive for high temperature sensor applications, they face a number of technical challenges. Optical grade sapphire fibers are difficult and

† First Author
* Corresponding Author,
E-mail : kcahn@chinju.ac.kr
TEL : +82-591-751-3352 ; **FAX** : +82-591-751-3359
Department of Mechanical Design Engineering, Chinju National University, 150 Chilam-dong, Chinju, Kyungnam 660-758, Korea. (Manuscript **Recevied** June 21, 2000; **Revised** December 21, 2000)

expensive to fabricate, and only available in short segments. Additionally, the sapphire fiber sensors utilized the fiber Fabry-Perot interferometer thus far developed show limited promise for multiplexing. The silica-based sensors described in Chang et al. (1994) and Lee and Taylor(1991) face similar limitations with regard to multiplexing.

In-fiber Bragg grating sensors, on the other hand, have excellent multiplexing potential and therefore it is worth investigating how Bragg grating structures can be used to develop high temperature strain sensors. The kinetics of Bragg grating growth in photosensitive fiber has shown that the temperature stability of in-fiber Bragg grating is different for Type Ⅰ and Type Ⅱ gratings, with Type Ⅰ and Ia gratings being limited to ~250 ℃ (Tsai et al., 1993 ; Ergogan et al., 1994) and Type Ⅱ grating being limited to ~800 ℃ (Miay et al., 1995 ; Poulson et al., 1995 ; Archambault et al, 1993). The temperature capability of Type II gratings rivals the operational temperature capabilities of traditional resistance and capacitance high temperature strain gages.

This paper describes a preliminary study of Bragg grating sensors etched into planar waveguide structures as a means of increasing the operational temperature range of the gratings, while at the same time preserving the multiplexing capability of Bragg grating sensors. These gratings are created by modifying the waveguide geometry instead of optical properties, and it may thus be possible to use them up to the softening point of silica (roughly 1200 ℃). The fabrication procedures for the proposed Bragg grating sensors can be very controllable, and show promise for cost effective mass production using the same technology employed by the microelectronics industry. These types of grating structures have been used in distributed feedback lasers, grating couplers, modulators, and filters, etc. (Suhara et al., 1986 ; Flanders et al, 1974 ; Schmidt et al., 1974 ; Hong et al., 1974 ; Lee et al., 1987). As a first step towards developing etched planar waveguide Bragg grating strain sensors, this paper develops fabrication techniques and mathematical model necessary for investing the optical and mechanical properties. The functional operation of these sensors is then tested in uniform temperature fields with temperatures up to 200 ℃. While this temperature range is modest in comparison with the stated target of 1200 ℃, it lays the foundation for future development.

2. Theoretical Analysis of Planar Waveguide Bragg Grating Sensor

This section provides the basic mathematical foundation that will be used to design and perform data analyses of the proposed planar waveguide etched grating sensor. This section starts by providing the expressions needed to calculate the propagation constants for the slab waveguide in terms of the waveguide geometric and optical properties. Then the coupled mode equations used to determine the grating properties are presented. The waveguide geometry of interest in this paper is illustrated in Fig. 1, and consists of a germanium doped SiO_2 core bounded by air above and pure SiO_2 below. This waveguide is fabricated on a silicon substrate. The refractive indices of air, core and cladding SiO_2 layers are denoted by n_1, n_2, and n_3, respectively and the core thickness is given by t_g. Also seen in Fig. 1 are the etched corrugations of pitch Λ and depth a.

The most important parameter in the design of Bragg grating in slab waveguides is the effective index. This effective index is found in the usual way (Yariv, 1973) by solving the wave equation and applying the continuity boundary conditions at the respective core/cladding interfaces of the

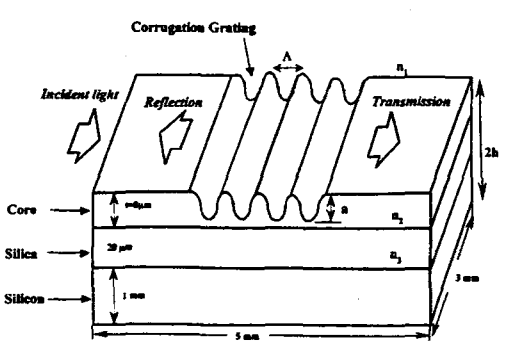

Fig. 1 Diagram of the slab waveguide with surface corrugation grating

waveguide shown in Fig. 1. The guided modes have a propagation constant β_s such that $k_0 n_3 < \beta_s < k_0 n_2$, where $n_1 < n_3$. This solution process leads to the following transcendental equation that yields the propagation constant:

$$\tanh t_g = \frac{p+q}{h(1-pq/h^2)} \tag{1}$$

where $h=(n_2^2k_0^2-\beta_s^2)^{1/2}$, $q=(\beta_s^2-n_1^2k_0^2)^{1/2}$, $p=(\beta_s^2-n_3^2k_0^2)^{1/2}$ and $k_0 \cong \bar{\omega}/c=2\pi/\lambda$. Given a set of refractive indices n_1, n_2, and n_3 and the waveguide thickness, t_g, of the planar waveguide, and the source wavelength, λ. Eq. (1) in general yields a number of solutions for the propagation constant, β_s. However, the source wavelength and the waveguide thickness are restricted in the present study such that only one propagation mode is supported, and therefore Eq. (1) has only one solution of interest. As a result, the effective index of the planar waveguide is given by $n_{eff}=\beta_s\lambda/2\pi$. The corrugated structure into the waveguide leads to a corresponding periodic perturbation of the refractive index distribution. Each groove of the grating acts like a weak mirror, and the cumulative effect of all of the weak reflectors results in a very strong combined reflection centered on what is known as the Bragg wavelength. The Bragg wavelength is related to the effective index calculated above and the grating period, Λ, by Yariv(1973)

$$\lambda_b = 2n_{eff}\Lambda \tag{2}$$

which when expressed in terms of the propagation constant is given by

$$\lambda_b = \beta_s\lambda\Lambda/2 \tag{3}$$

where λ_b is the Bragg wavelength and λ is the central wavelength of the optical source. The fraction of power couple to the backward-propagation mode $(-\beta_s)$, i. e. the grating reflectivity is given by (Yariv, 1973)

$$\Re_{max} = \tanh^2(\kappa L) \tag{4}$$

where L is the length of the Bragg grating and the coupling coefficient κ is given by (Yariv, 1973)

$$\kappa = -\frac{2\pi^2}{3\lambda}\frac{(n_2^2-n_1^2)}{n_2}\left(\frac{a}{t_g}\right)^3\left[1+\frac{3}{2\pi}\frac{\lambda/a}{(n_2^2-n_1^2)^{1/2}}+\frac{3}{4\pi^2}\frac{(\lambda/a)^2}{(n_2^2-n_1^2)}\right. \tag{5}$$

where l is the integer number of Bragg diffraction orders. Equations (1) through (5) are used to perform preliminary design of the planar waveguide grating sensor, and to guide the experimental program.

A change in the temperature of the planar waveguide causes a shift in the Bragg wavelength due to thermal expansion, and the thermo-optic change in the effective index. The temperature-induced fractional wavelength shift is given by (Morey et al., 1989)

$$\frac{\Delta\lambda_b}{\lambda_b} = (1-p_e)\varepsilon_g + \xi\Delta T \tag{6}$$

where ε_g is the thermal strain in the guiding layer of the waveguide, $P_e=0.21$ is the strain-optic coefficient for silica, and ξ is the thermo-optic coefficient of the germanium-doped silica core (Takahashi et al., 1979). The coefficient of thermal expansion for fused silica at temperatures between 0℃ and 500 ℃ can be given by (Malitson, 1965)

$$\alpha_1(T) = a_1 + a_2T + a_3T^2 \tag{7}$$

where $a_1=0.395\times10^{-6}$/℃, $a_2=1.282\times10^{-6}$/℃, $a_3=-1.7\times10^{-6}$/℃. Similarly, the change in refractive index in the form of the differential variation for fused silica at given temperature between −200 ℃ and 640 ℃ is given by (Waxler et al., 1973)

$$n_{eff}\xi = \frac{dn(T)}{dT} = b_1 + b_2T + b_3T^2 \tag{8}$$

where $b_1=8.16638\times10^{-6}$, $b_2=1.04124\times10^{-8}$, $b_3=-5.59781\times10^{-12}$. This functional form for the temperature dependence of the core and cladding refractive indices are used with Eqs. (1) through (3) to calculate the temperature dependent effective thermo-optic response of the waveguide.

The slab waveguide is composed of two layers of materials with different Young's modulii and coefficients of thermal expansion. As a result, a change in temperature can cause a combination of expression of expansion and warping. The degree of warpage will depend on the mismatch in thermomechanical properties and difference in thicknesses. This type of mechanical system can be analyzed using the Classical Laminated Plate

Table 1 Materials properties of the silica and silicon

Materials	Thermal Expansion Coefficient, α(/℃)	Thermo-Optic Coefficient, ξ(/℃)	Young's Modulus, E(GPa)	Poisson's Ratio, ν
Silica	Eq. (7)	Eq. (8)	73	0.19
Silicon	Eq. (10)	—	190	0.27

Theory (CLPT) often utilized in the analysis of laminated composites structures (Okada and Tokumaru, 1984). The incarnation of the CLPT used here is based on the following basic assumptions: (1) the layers within a laminate are considered perfectly bonded, (2) each layer is homogeneous, (3) each layer experiences plane stress conditions only, (4) plane sections remain plane. Following the CLPT approach, the strains on the surface of the waveguide is given by

$$\{\varepsilon\}=\{\bar{\varepsilon}^0\}+z\{\bar{k}\} \tag{9}$$

where $\{\bar{\varepsilon}^0\}$ is the global mid-plane strain, $\{\bar{k}\}$ is the global curvature, and z is the distance from the laminate mid-plane to the plane on which the strain is to be calculated. As is given the coefficient of the fused silica above, the coefficient of thermal expansion for silicon at temperatures between −153 ℃ and 1227 ℃ can be given by Petersen(1982)

$$\alpha_2(T)=3.725\times10^{-6}[1-\exp(-5.88\times10^{-3}(T+149))]+5.548\times10^{-6}T \tag{10}$$

The CLPT can provide details of how the mid-plane strains and curvatures are derived in terms of the Young's modulii, coefficients of thermal expansion and thicknesses of SiO_2 waveguide and the silicon substrates. This analysis assumes that both the silica and silicon has isotropic mechanical properties (Table 1 provides the relevant properties (Kelly, 1973 ; Izawa et al., 1981). Even though silicon is known to be anisotropic, the isotropy assumption is sufficient for the present analysis.

3. Experiment

3.1 Fabrication of sensor

The planar waveguides used in these studies are fabricated by Photonics Integrated Research Inc. (PIRI) using hydrolysis deposition(Hill et al., 1978). These waveguides are originally manufactured with an 8 μm thick germanium doped silica core with a 20 μm silica undercladding sitting on top of a 1 mm thick silicon substrate. The refractive indices of the core layer and undercladding layer are 1.4495 and 1.4452 measured at 1.55 μm wavelength, respectively. The waveguide blank is diced parallel or perpendicular to the straight edge of the silicon substrate into 3 mm long x 5 mm wide waveguides.

Bragg gratings are produced in the planar waveguides using photoresist based optical lithography techniques. This process starts by first spin coating a 50 % dilution of Shipley S1400-17 photoresist onto the surface of the waveguide at 6000 rev/min for 30 seconds. The resulting ~220 nm layer of photoresist is soft baked for 35 min at 96 ℃ to ensure complete removal of thinning solvents. A phase mask printing method is then used to fabricate the Bragg gratings (Morey et al., 1989 ; Moreau, 1988). A phase mask is used to produce two equal amplitude interfering optical beams, as shown in Fig. 2. The interfering pattern is expanded in size so that interference occurs in a 2 mm smaller diameter circular region. Grating are typically written in the planar waveguide coated by exposing the photoresist to the 244 nm UV light for 5 sec to 8 sec with laser powers ranging from 2 mW to 3 mW. The phase mask used in this study had a pitch of 0.5278 μm and 15.4 % transmission of zeroith order diffraction. This phase mask pitch corresponds to a Bragg wavelength somewhat near 1550 nm, depending on the effective index of the waveguide. Once exposed, the waveguides are baked for 12 min at 120 ℃.

Also seen in Fig. 3 is the next step at which the grating fabrication process involves developing the photoresist for typically 12 sec with a devel-

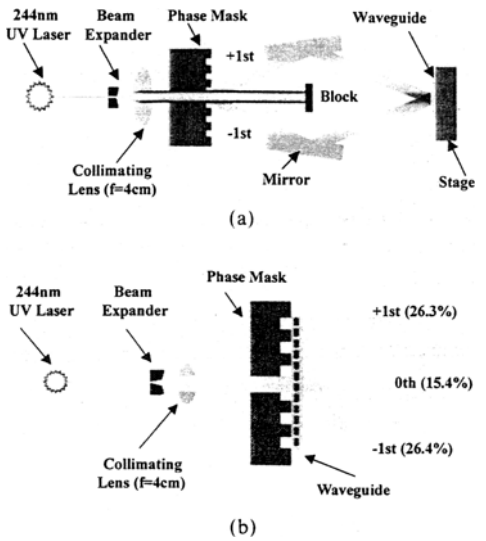

Fig. 2 The schematics of the optical phase mask printing setup for fabrication of Bragg grating

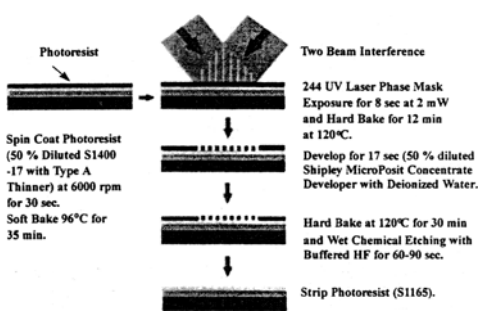

Fig. 3 The lithographic procedures of fabrication of the grating on the waveguide

oper made of one part Shipley Microposit Concentrate and one part deionized water to form resist gratings. The waveguide is then rinsed in deionized water for 30 sec and then blown dry with nitrogen gas. After developing, the substrates are baked for 30 min at 120 ℃, and then are wet-chemically etched for 75 seconds to a depth of 130 nm to 200 nm using bufferd HF (Veselka et al, 1986). Next, the photoresist is stripped using solvents such as Shipley S1165 remover or acetone. The gratings investigated here typically have a 537.8 nm period as measured using an Atomic Force Microscope (AFM) shown in Fig. 4(a) and/or an Environmental Scanning Electron Microscope (ESEM) shown in Fig. 4b. It

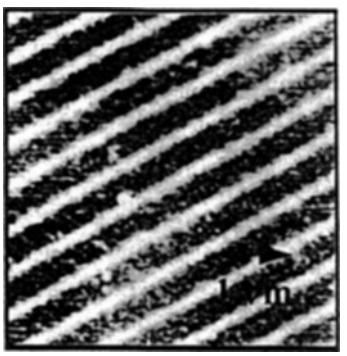

(a) Atomic force microscope

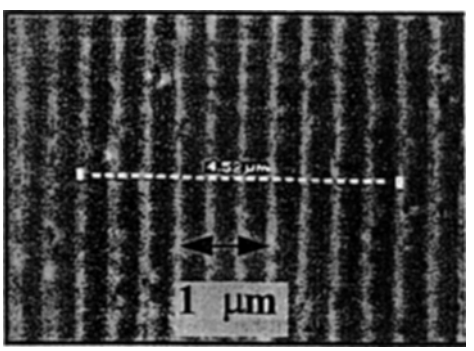

(b) Environmental scanning electron microscope

Fig. 4 The photograph of the etched Bragg grating formed on the waveguide

was very difficult to obtain a homogeneous grating structure because the zeroith order diffracted beam from the phase mask caused unwanted fringe patterns, resulting from multiple reflections between the planar waveguide and the phase mask. It is noted that the distance between the phase mask and the planar waveguide has to be minimized without causing the damage of the phase mask to minimize the above noted multiple reflections.

The final step in the grating sensor fabrication process is to prepare the edges of the waveguides to facilitate coupling light into the sensor and to provide for visual inspection. This is done by first cleaning the diced waveguide with solvents (acetone and methanol) and then blow drying it with nitrogen gas. The waveguide is mounted on a jig with the heat-melt wax and is polished using 1 micron and 0.3 micron aluminum oxide on a polishing wheel rotating at 1500 rev/min. The polishing is done using 0.1 micron diamond sheet.

Visual inspection using a transmission optical microscope is used to control the surface roughness of the waveguide facet. Finally, the polished waveguide is thoroughly cleaned in acetone for 30 min at 100 ℃ to remove the residual wax.

3.2 Butt coupling techniques

The etched grating sensor is interrogated by using a single mode optical fiber to carry the light to and from the sensors. This means that efficient fiber to waveguide coupling techniques must be used. Tolerancing typical of lowest insertion losses are offset by less than ± 2 μm and an angular misalignment by less than 0.5°. The butt coupling technique used to achieve the efficient fiber to waveguide coupling is shown schematically in Fig. 5. Amplified Spontaneous Emission (ASE) from an Erbium Doped Fiber Amplifier (EDFA) is launched into one arm of a 3 dB coupler fabricated with optical fiber having a mode field diameter of 9.5 μm. One arm of the coupler is index matched to prevent back reflection and the other arm is butt coupled into the waveguide. Light reflected from the waveguide is directed by the 2×2 coupler to an optical spectrum analyzer. The first step of the alignment process involves replacing the EDFA with a Helium Neon laser and imaging the transmitted near-field beam appearing at the back facet of the waveguide with a CCD camera. The Helium Neon laser is used because its wavelength falls within the spectral bandwidth of the CCD camera. The optical fiber and the planar waveguide are first aligned visually, and then a five degree of freedom monopositioning stage is used to adjust the location and orientation of the waveguide, while viewing the near field image on a video monitor. This process is stopped when the near-field image intensity is maximized, and its shape is symmetric and centrally located. The He-Ne laser is then replaced with an EDFA, and the gap between the optical fiber and waveguide is reduced while monitoring the reflected spectrum in the optical spectrum analyzer. Optimum positioning is achieved when the spectrum associated with the air gap Fabry-Perot interferometer formed between the optical fiber and the waveguide facet is minimized. Index matching liquid (refractive index, 1.4587, Cargille Company) is applied to the back facet of the waveguide sensor to prevent a Fabry-Perot cavity from forming between the two waveguide facets.

3.3 Grating characterization

The exact center wavelength of the grating reflectivity will vary with the effective index of the guided mode, which itself depends on the waveguide dimensions. As part of the grating evaluation process, the effective indices of the slab waveguides were measured using the intermodal spacing in the optical spectra produced by a Fabry-Perot interferometer purposefully formed between the two facets of the waveguide. This effective index is given by

$$n_{eff}=\lambda_o^2/(2\delta\lambda L_w) \tag{11}$$

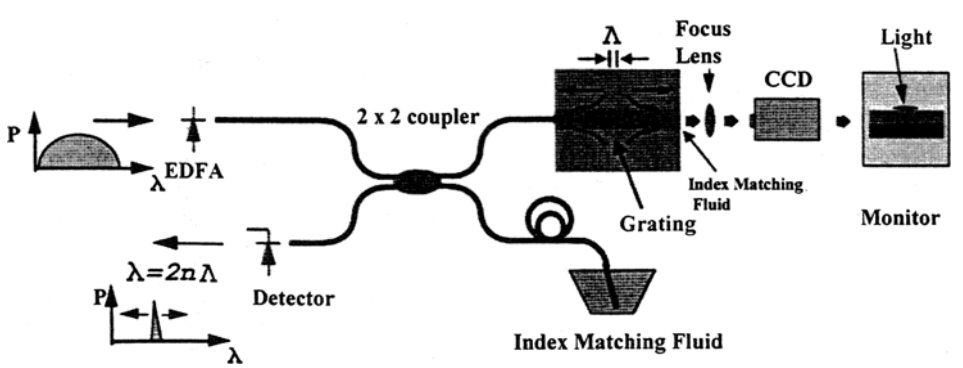

Fig. 5 The schematic of the coupling technique used to investigate spectral characteristics of planar waveguide Bragg gratings

where λ_0 is the peak emission wavelength, $\delta\lambda$ is the intermodal spacing of the waveguide cavity and L_w is the length of the cavity. The intermodal spacing of the waveguide cavity is measured using the EDFA in the arrangement shown in Fig. 5. In this case, however, steps are taken to promote Fabry-Perot interference between the two waveguide facets. This involves keeping a ~ 1 μm gap between the optical fiber lead and front facet, and not using an index matching liquid on the back facet. The resulting optical spectrum is viewed using an Advantest, Model Q8347 optical spectrum analyzer. This particular OSA enables the intermode spacing measurements with 0.007 nm wavelength resolution.

The reflected spectrum produced by a grating 2 mm long, 200 nm deep (typical values) etched into a planar waveguide was measured with the optical spectrum analyzer as well. The reflected spectrum of the reflection from the planar waveguide gratings generally appeared bifurcated due to geometry-induced birefringence. Therefore, an output fiber polarizer is used to isolate the Bragg condition from one polarization mode. In order to examine temperature sensing performance of the etched planar waveguide Bragg grating sensor, the planar waveguide Bragg grating was heated with temperature ranging from 20 ℃ to 200 ℃ using the heating tape which fold the translating block mounting the planar waveguide.

4. Results and Discussion

Several waveguide sensors were fabricated using the techniques described in Sec. 3. Table 2 provides the measured and calculated values of the effective index of the waveguide at room temperature for four of these waveguides. The measured values are determined using Eq. (11) and the calculated values are determined using the results of Eq. (1). Note that these calculations were performed with $n_1=1.0$, $n_2=1.4495$, $n_3=1.4452$, $t_g=8.0$ μm, and $\lambda_0=1550$ nm. Table 2 also shows the waveguide length (distance between facets), the measured intermodal spacing, the Bragg wavelength calculated using Eq. (3), as well as the measured Bragg wavelength. This data shows that the measured effective indices and Bragg wavelengths of the slab waveguide predicted values agree to within 0.21 %. This difference is most likely attributable to the measurement errors imposed by the spectrum analyzer resolution and variability in the waveguide thickness. Nevertheless, the data in Table 2 shows that the models developed in Sec. 2 are sufficient for the purposes of waveguide sensor design and analysis.

Figure 6 shows the reflected spectrum produced by a grating 2 mm long, 200 nm deep (typical values) etched into a planar waveguide. The reflected spectrum of the reflection from the planar waveguide gratings generally appeared bifurcated due to geometry-induced birefringence. Therefore, an output fiber polarizer is used to isolate the Bragg condition from one polarization mode. However, the birefringent bifurcation of the waveguide in the present study disappeared at high temperature during the temperature measurement. Typical values for the grating bandwidth and reflectivity are 0.2 nm and $\sim$0.7 %, respective-

Table 2 Summary of the values of the effective refractive indices measured from the waveguides

Sensor	Waveguide Length L_w (mm)	Intermode Spacing $\delta\lambda_o$ (nm)	Measured Effective Refractive Index N_{eff}	Predicted Effective Refractive Index n_{eff}	Predicted Bragg Wavelength λ_b (nm)	Measured Bragg Wavelength λ_b (nm)
1	4.78	0.174	1.4452	1.4464	1555.79	1552.57
2	4.79	0.173	1.4495	1.4464	1555.79	1556.55
3	3.19	0.260	1.4483	1.4464	1555.79	1552.65
4	4.81	0.172	1.4481	1. 4464	1555.79	1552.44

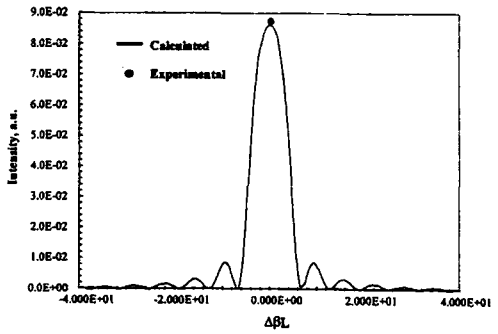

Fig. 6 The reflectivity of the etched planar waveguide Bragg grating sensor

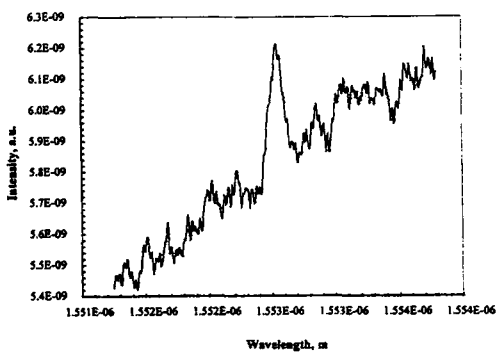

Fig. 7 Reflection spectrum of etched Bragg grating formed on the planar slab waveguide

ly. To compare the calculated and measured alues only one experimental point could be shown because the reflectivity could be predicted only at room temperature although the experimental results obtained at elevated temperature were available. The reflectivity of this grating calculated with Eq. (4) and L=2.0 mm and a=200 nm is 7.1 %, which agrees with experiments to within 1.4 %. Also noticeable in the spectrum provided in Fig. 7, is a small magnitude periodic artifact which is due to the Fabry-Perot cavity formed between the front and back facets of the waveguide. Although this effect was minimized by applying index matching fluid (Cargille, the refractive index, 1.4587) to the back facet of the planar waveguide, a small amount of light still resonated in the cavity due to imperfect index matching. Angle polishing the back facet of the waveguide is planned for future research to reduce Fabry-Perot effects to a larger degree.

The calculated result using the equation above

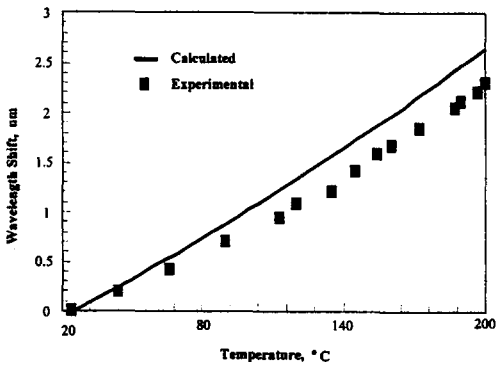

Fig. 8 Comparison of shift in Bragg wavelength induced by temperature change with theory with nonlinear effect

with specified coefficients is 0.0137 nm/℃. The measured sensitivity is 3.6 % lower than the calculated value. The material properties in Table 1 are used with Eq. (9) to calculate the thermal strain in the core of the waveguide. This strain is then substituted into Eq. (8) to estimate the thermally induced change in the Bragg wavelength. These calculations lead to a proportionality factor between the change in wavelength and temperature of 0.0137 nm/℃. For comparison, the proportionality factor for a ~1550 nm photorefractive grating written in an optical fiber is 0. 0132 nm/℃.

Figure 8 provides a graph of Bragg wavelength as a function of temperature measured using a spectrum analyzer. The solid line in this figure is the wavelength response predicted using Eq. (9). Typically, the temperature-induced fractional Bragg wavelength shift measured in this experiment varied nonlinearly and is 3.6 % less than the predicted slope. Figure 9 shows the reflectivity at the Bragg wavelength as a function of temperature. As seen in this figure, the reflectivity increases at 44 ℃. Also, the reflectivity is decreased up to about 100 ℃. Hoewever, the reflectivity remains stable from 100 ℃. The origin of this effect is not clear, but a silica overcladding would likely reduce the variability. The spectral bandwidth of the grating was also measured as a function of temperature, with no significant variations observed as shown in Fig. 10. With regard to Fig. 10, the resolution of the measurement

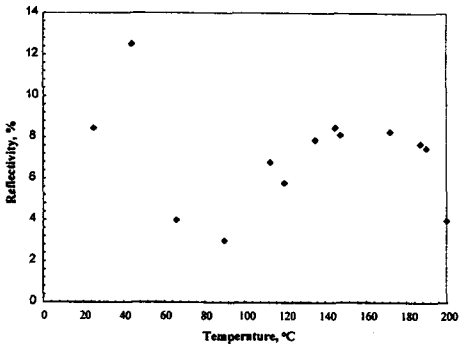

Fig. 9 Reflectivity of Bragg wavelength in etched planar waveguide grating sensor at elevated temperature

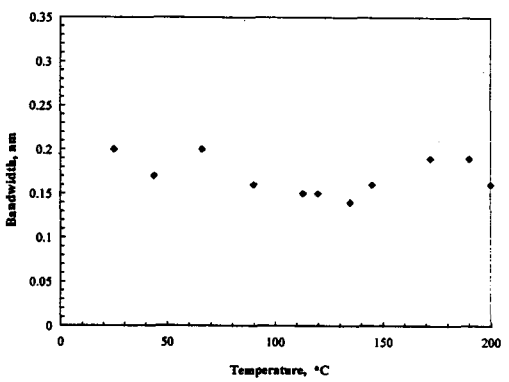

Fig. 10 Bandwidth of Bragg wavelength in etched planar waveguide grating sensor at elevated temperature

technique was 0.007nm. This allowed the optical spectrum analyzer (HP Advantest, Model Q8347) to read 0.032nm/℃ sensitivity of the sensor.

5. Conclusions

A temperature sensor based on the etched planar waveguide Bragg grating was developed and its performance was explored using theoretical and experimental methods. The planar waveguide is designed and fabricated using optical lithography and wet chemical etching. An efficient butt coupled optical fiber was used to examine the spectral characteristics of the grating sensor, and to investigate the grating parameters. Classical laminated plate theory used with temperature dependent thermo-optic coefficient was combined in a simple model for the grating temperature response to predict the response of the temperature sensor. These theoretical predictions showed that the non-linear behavior of the sensor can be important at higher temperatures. This paper has demonstrated only the first step in developing high temperature strain gages and temperature sensors. Much work is still needed in device design and fabrication. This should include transition from planar to channel waveguides to minimize insertion loss. Methods of angle polishing the waveguide facets and for adding an amorphous silica overcladding should also be incorporated into the sensor fabrication. Only then will tests at extreme temperatures be possible. Even so, the results in this paper provide the fabrication and analysis frame work needed for continued development.

References

Archambault, J. L., Reekie, L. and Russel, P. St. J., 1993, "100 % Reflectivity Bragg Reflectors Produced in Optical Fibers by Using Single Excimer Pulses," *Electronics Letters*, Vol. 29, pp. 453~454.

Chang, C. C., Sagrario, D., Job, L. and Sirkis, J. S., 1994, "Using Standard Interferometric Sensors for High Temperature Strain Measurements," *SPIE* Vol. 2191, pp. 482~486.

Dils, R. R., 1983, *Journal of Applied Physics*, 84, 1198.

Ergogan, T., Mizrahi, V., Lamaire, P. J. and Monroe, D., 1994, "Decay of Ultraviolet-Induced Fiber Bragg Gratings," *Journal of Applied Physics*, Vol. 76, pp. 73~80.

Flanders, D. C., Kogelnik, H., Schmidt, R. V. and Shank, C. V., 1974, "Grating Filters for Thin -Film Optical Waveguide," *Applied Physics Letters*, Vol. 24, No. 4, pp. 194~196.

Harting, R, 1975, "Evaluation of a Capacitive Strain Measuring System for Use to 1500 ℃," *ISA 75251*, pp. 289~297.

Hill, K. O. Fugii, Y., Johnson, D. C. and Kawasaki, B. S., 1978, "Photosensitivity on Optical Fiber Waveguides: Application to Reflection Filter Fabrication," *Applied Physics Letters*, Vol.

32, pp. 647~649.

Hong, C. S., Shellan, J. B., Livanos, A. C., Yariv, A. and Katzir, A., 1974, "Broad-Band Grating Filters for Thin-Film Optical Waveguide," *Applied Physics Letters*, Vol. 31, No. 4, pp. 276~278.

Hudson, L. D., 1989, "Recinet Experiences With Elevated-Temperature Foil Strain Gages With Application to Thin-Gage Materials," *Proc. 6th Annual Conf. On Hostile Environments and High Temperature Measurements, Society for Experimental Mechanics*, pp. 68~81.

Izawa, T., More, H., Murakami, Y. and Shimizu, N., 1981, "Deposited Silica Waveguide for Integrated Optical Circuits," *Applied Physics Letters*, Vol. 38, No. 7, pp. 483~485.

Kelly, A., 1973, *Strong Solids*, 2nd Ed. Oxford England: Clarendon.

Lee, C. E. and Taylor, H. F., 1991, *IEEE Journal of Lightwave Technology*, 9, 129.

Lee, H. J., Henry, C. H., Kazarinov, R. F. and Orlowsky, K. J., 1987, "Low Loss Bragg Reflectors on SiO_2-Si_3N_4-SiO_2 Rib Waveguides," *Applied Optics*, Vol. 26, No. 13, pp. 2618~2620.

Lei, J. F., Okimura, H. and Brittain, J. O., 1989, "Evaluation of Some Thin Film Transition Metal Compounds for High Temperature Resistance Strain Gauge Application," *Materials Science Engineering*, A111, pp. 145~154.

Malitson, I. H., 1965, "Interspecimen Comparison of the Refractive Index of Fused Silica," *J. Opt. Soc. America*, Vol. 55, No. 10, pp. 1205~1210.

Miay, P., Bernage, P., Douay, M., Taunay, T., Sie, W. X., Martinelli, G., Bayon, H. F., Poignant, H. and Devevaque, E., 1995, "Bragg Grating Photoinscription Within Various Types of Fibers and Glasses," *Proceedings of Photosensitivity and Quadratic Nonlinearity in Glass Waveguides: Fundamentals and Applications, OSA Technical Digest*, Vol. 22, pp. 66~69.

Moreau, W. M., 1988, Semiconductor Lithography: Principles, Practices, and Materials, New York: Plenum Press, pp. 646~650.

Morey, W. W., Meltz, G. and Glenn, W. H., 1989, "Fiber Optic Bragg Grating Sensors," *Fiber Optic and Laser Sensors* Ⅶ, *SPIE* Vol. 1169, pp. 98~107.

Noltingk, B. E., 1974, "Measuring Static Strains at High Temperatures," *Experimental Mechanics*, Vol. 15, No. 10, pp. 420~423.

Norris, E. B. and Yeakley, L. M., 1976, "Development of High-Temperature Capacitance Strain Gages," *ISA National Technical Information Service*, PB 257, January.

Okada, Y., Tokumaru, Y., 1984, *J. Applied Physics*, Vol. 56, No. 2, pp. 314~320.

Petersen, K. E., 1982, *Proceedings of IEEE*, Vol. 70, pp. 420~ ? ? ? .

Poulsen, C. V., 1995, "Thermal Stability of Direct UV-Written Channel Waveguides," *Proceedings of Photosensitivity and Quadratic Nonlinearity in Glass Waveguides: Fundamentals and Applications, OSA Technical Digest*, Vol. 22, pp. 100~103.

Schmidt, R. V., Flanders, D. C., Shank, C. V. and Standley, R. D., 1974, "Narrow-Band Grating Filters for Thin-Film Optical Waveguide," *Applied Physics Letters*, Vol. 25, No. 11, pp. 651~652.

Stange, W. A., 1983, "Advanced Techniques for Measurement of Strain and Temperature in a Turbine Engine," *AIAA/SAE/ASME 19th Jet Propulsion Conference.*, Seattle, WA, AIAA-83-1296.

Suhara, T. and Nishihara, H., 1986, "Integrated Optics Component and Devices Using Periodic Structures," *IEEE Journal of Quantum Electronics*, Vol. 22, No. 6, pp. 845~867.

Takahashi, S. and Shibata, S., 1979, "Thermal Variation of Attenuation for Optical Fibers," *Journal of Non-Crystalline Solids*, Vol. 30, pp. 359~370.

Tsai, T. E., Friebele, E. J. and Griscom, D. L., 1993, "Thermal Stability of Photoinduced Gratings and Parametric Centers in Ge- and Ge/P-Doped Silica Optical Fibers," *Optics Letters*, Vol. 18, pp. 935~937.

Veselka, J. J. and Korothy, S. K., 1986, "Optimization of Ti:$LiNbO_3$ Optical Waveguides and Directional Couplers Switches for 1.56 Micrometer Wavelength," *IEEE Journal of Quantum Electronics*, Vol. 22, pp. 930~938.

Wang, A., Wang, G. Z., Gollapudi, S., May, R.

G., Murphy, K. A. and Claus, R. O., 1992, "Advances in Sapphire Optical Fiber Sensors," *Proceedings of. Fiber Optic Smart Structures and Skins V, SPIE*, Vol. 1798, pp. 56~65.

Waxler, M., Cleek, G. W., 1973, "The Effect of Temperature and Pressure on the Refractive Index of Some Sxide Glasses, " *J. Res. Nat. Bureau of Stan.* Vol. 77A, No. 6, pp. 755~763.

Wu, T., Ma. L. C. and Zhao, L. B., 1981, "Development of Temperature-Compensated Resistance Strain Gages for Use to 700 ℃," *Experimental Mechanics*, Vol. 21, No. 3, pp. 117~123.

Yariv, A., 1973, "Coupled-Mode Theory for Guided-Wave Optics," *IEEE Journal of Quantum Electronics*, Vol. 9, pp. 919~933.